The collective and quantum nature of proton transfer in the cyclic water tetramer on NaCl(001)

Yexin Feng, Zhichang Wang, Jing Guo, Ji Chen, En-Ge Wang, Ying Jiang, and Xin-Zheng Li

Citation: The Journal of Chemical Physics **148**, 102329 (2018);
View online: https://doi.org/10.1063/1.5004737
View Table of Contents: http://aip.scitation.org/toc/jcp/148/10
Published by the American Institute of Physics

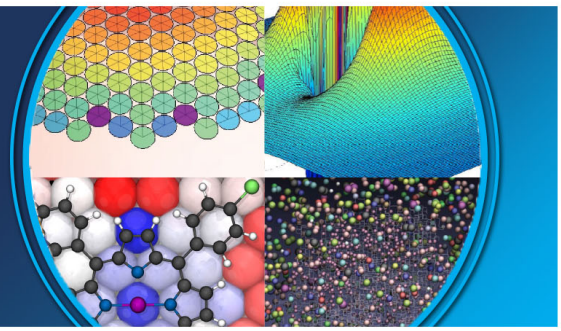

The collective and quantum nature of proton transfer in the cyclic water tetramer on NaCl(001)

Yexin Feng,[1,2] Zhichang Wang,[1] Jing Guo,[1] Ji Chen,[1] En-Ge Wang,[1,3] Ying Jiang,[1,4,a)] and Xin-Zheng Li[1,4,a)]

[1]*International Center for Quantum Materials and School of Physics, Peking University, Beijing 100871, People's Republic of China*
[2]*School of Physics and Electronics, Hunan University, Changsha 410082, People's Republic of China*
[3]*CAS Center for Excellence in Topological Quantum Computation, University of Chinese Academy of Sciences, Beijing 100190, People's Republic of China*
[4]*Collaborative Innovation Center of Quantum Matter, Beijing 100871, People's Republic of China*

(Received 15 September 2017; accepted 3 December 2017; published online 22 December 2017)

Proton tunneling is an elementary process in the dynamics of hydrogen-bonded systems. Collective tunneling is known to exist for a long time. Atomistic investigations of this mechanism in realistic systems, however, are scarce. Using a combination of *ab initio* theoretical and high-resolution experimental methods, we investigate the role played by the protons on the chirality switching of a water tetramer on NaCl(001). Our scanning tunneling spectroscopies show that partial deuteration of the H_2O tetramer with only one D_2O leads to a significant suppression of the chirality switching rate at a cryogenic temperature (T), indicating that the chirality switches by tunneling in a concerted manner. Theoretical simulations, in the meantime, support this picture by presenting a much smaller free-energy barrier for the translational collective proton tunneling mode than other chirality switching modes at low T. During this analysis, the virial energy provides a reasonable estimator for the description of the nuclear quantum effects when a traditional thermodynamic integration method cannot be used, which could be employed in future studies of similar problems. Given the high-dimensional nature of realistic systems and the topology of the hydrogen-bonded network, collective proton tunneling may exist more ubiquitously than expected. Systems of this kind can serve as ideal platforms for studies of this mechanism, easily accessible to high-resolution experimental measurements. *Published by AIP Publishing.* https://doi.org/10.1063/1.5004737

I. INTRODUCTION

Hydrogen (H)-bonding interaction is an important type of inter-molecular interaction in many physical, chemical, and biological systems, e.g., the binding of DNA base pairs,[1–3] the phase transition of high-pressure ice and super-ionic water,[4–7] the proton exchange through membranes,[8–11] the functioning of enzymes,[12–17] etc. Due to the light mass of H, many of these systems and problems are highly quantum mechanical in nature.[3,5,14–26] As a consequence, accurately accounting for the nuclear quantum effects (NQEs) has become a more and more important issue in their theoretical descriptions and experimental characterizations nowadays. To name a few examples, the agreement between theories and experiments on the momentum distribution of protons and the vibrational dynamics in liquid water and bulk ice can be substantially improved after including NQEs in the *ab initio* simulations.[19–23] The NQEs were vital in the auto-ionization of liquid water.[24] In descriptions of the strength of H-bonding interactions, the NQEs were indispensable in the theoretical simulations and detectable in experiments.[25–28]

Proton transfer is an elementary process in H-bonded systems, first suggested by von Grotthuss more than 200 years ago,[29,30] before Avogadro found that a water molecule is H_2O. Under the classical approximation, proton transfer happens through thermal hopping. But the quantum nature of the nuclei can also impact on this process in terms of tunneling and zero-point motion. When zero-point energy can wash out the classical proton transfer energy barrier, the protons delocalize along the H-bonds and NQEs induce qualitatively different classical and quantum structures.[5,18,31] When zero-point energy is not large enough to induce completely delocalized protons, quantum tunneling becomes the dominant NQEs.[15–17,32] In quantum dynamics, this is a subject of intense research.[33–39] The simplest process happens through single (stepwise) proton tunneling from one site to another along the H-bond.[5,14–17,32–38] Parallel to this single proton tunneling, multiple proton tunneling also exists,[39,40] and sometimes they happen in a collective (or concerted) manner. This collective proton tunneling was first proposed in molecular dimers, such as H-bonded carboxylic acid dimer and formic acid dimer.[40–43] Physics behind it in terms of the competition between NQEs in different dimensions is clearly non-trivial.[42] Systematic investigations of this mechanism using *ab initio* simulations or high-resolution experiments, however, are scarce.

One exception is the proton transfer within a hexagonal water ring in ice I_h at low temperature (T).[44–47] In this system, incoherent quasielastic neutron scattering measurements have

a)Authors to whom correspondence should be addressed: yjiang@pku.edu.cn and xzli@pku.edu.cn

shown the existence of non-Arrhenius H jump and large isotope effects between H and deuterium (D), implying that the concerted proton tunneling plays an important role.[44] Using *ab initio* path-integral molecular dynamics (PIMD), Drechsel-Grau and Marx have pointed out that NQEs can reduce the activation barrier of the collective proton transfer from ~1.0 eV to ~0.2 eV at 50 K and six protons in the ring-like topologies behave like a delocalized quasiparticle at the transition state (TS) via collective tunneling along the proton transfer coordinate.[45] Upon isotopic substitution of one H_2O by D_2O, quantum simulations from the same group further showed that a Zundel-like complex exists at the TS which localizes the ionic defects and thus inhibits perfectly correlated proton tunneling.[46,47] Direct experimental characterizations of this process, especially those with atomic-level spatial resolution, however, are still lacking.

Another example for the demonstration of this concerted proton tunneling resides on the water tetramer on NaCl(001), when Meng and co-workers found that the chirality switching of the water tetramer can be controlled by a chlorine (Cl)-terminated tip of scanning tunneling microscope (STM).[48–50] This chirality switching was induced because of the rearrangement of the protons in the water tetramer.[48] The non-Arrhenius dynamics means that the chirality switching happens through tunneling.[48] The switching rate changes non-monotonically with tip height in the experiment, and its trend agrees with that of the collective proton transfer energy barrier. Besides this, it was also found that as the tip moves away from the center of the tetramer, the switching rate rapidly drops. All these findings suggest a translational collective proton tunneling mechanism. However, the effect of the partial isotopic substitution on the chirality switching, which is critical for the confirmation of the concerted proton tunneling mechanism,[46,48,50] has not been measured experimentally. What is more, it is also demanding to explore the atomistic details of the tunneling process with quantum simulations. These theoretical simulations were not reported in Ref. 48 either.

In this paper, we report additional experimental observations focusing on partial isotopic substitution and new classical/quantum simulations of the different chirality switching mechanisms of the water tetramer to understand the experimental observations. By manipulating individual H_2O and D_2O molecules on the NaCl(001) surface in the STM experiments,[49] we construct water tetramer ($4H_2O$), partially deuterated tetramer ($3H_2O$+D_2O), and fully deuterated tetramer ($4D_2O$). The H_2O and D_2O molecules were distinguished by tip-enhanced inelastic electron tunneling spectroscopy (IETS).[28] We found that upon partial deuteration of water tetramers (replacing just one H_2O with one D_2O), the switching rate is largely suppressed, almost to the same level as the case of full deuteration. This provides an experimental evidence for the breakdown of the concerted proton tunneling upon partial deuteration, as suggested by Drechsel-Grau and Marx for the water hexagonal ring in ice I_h in Ref. 46. Using classical and quantum *ab initio* simulations, we then carried out an atomistic study of this chirality switching process by investigating different mechanisms including translational concerted (collective) proton tunneling and collective/stepwise water molecule rotations. Our calculated static barriers with the climbing image nudged elastic band (cNEB) method show that the stepwise rotation of water molecules is more facile in the classical limit. *Ab initio* PIMD simulations, however, demonstrate a much lower quantum barrier (<0.2 eV) for the collective proton transfer mode at low T (50 K). These results come about because NQEs have different influences on different chirality switching pathways at low Ts. Obvious proton delocalization between the two degenerate states of the H-bond over a wide range of the reaction coordinate substantially reduces the free-energy barrier for collective proton transfer. For chirality switching based on water molecule rotations, this effect is much weaker. Based on one practical quantum transition state theory (QTST), T-dependent chirality switching rates and the isotope effects were calculated down to 50 K, which qualitatively explained the experimental results. These findings provide atomistic details for collective proton tunneling in a realistic system, which is accessible to experimental characterizations.

II. METHODS

The experiments were performed with an ultrahigh vacuum cryogenic STM (Createc) at 5 K. The preparation of the sample and Cl-terminated tip was described in Refs. 48 and 49. The partial deuterated water tetramer ($3H_2O$+D_2O) is constructed by manipulating four individual water molecules (three H_2O monomers and one D_2O monomer) with the Cl-terminated tip at a gap set with V = 10 mV, I = 150 pA. The H_2O and D_2O molecules could be distinguished by reference to the frequency of the O–H/D stretching mode with the recently developed tip-enhanced IETS.[28] Using scanning tunneling spectroscopy, dI/dV and d^2I/dV^2 spectra were acquired simultaneously using lock-in detection of the tunneling current by adding a 5-7 mV rms modulation at 237 Hz to the sample bias. The time trace of the tunneling current during chirality switching was recorded to extract the switching rate, and the corresponding experimental method was discussed in detail in Ref. 48. The bias voltage refers to the sample voltage with respect to the tip. All the STM topographic images were obtained in the constant-current mode.

The theoretical simulations were performed using the Vienna *Ab initio* Simulation Package (VASP),[51,52] with an in house implementation of the *ab initio* constrained molecular dynamics (MD) and constrained centroid PIMD methods.[53,54] With *ab initio* MD, the classical thermal effects of the nuclei were addressed as the electronic structures were calculated on-the-fly. With *ab initio* PIMD, the NQEs were added on the same footing. Therefore, comparisons between the *ab initio* MD and PIMD simulations allow the NQEs to be analyzed in a very clean manner.[18,53–60] The atomic structure of the system used is similar to Ref. 48, a (2 × 2) NaCl unit cell on a $\begin{pmatrix} 3 & 1 \\ 1 & 3 \end{pmatrix}$ superstructure of the Au(111) substrate with a residual strain of about 5% was used, which contains a bilayer NaCl(001) lattice on top of four-layer Au(111). The bottom layer of the NaCl and the Au substrates was fixed during geometry relaxations. The thickness of a vacuum slab was larger than 12 Å in all simulations. We performed the cNEB calculations to obtain the static energy profiles of different proton

transfer modes for the chirality switching of water tetramers.[61] Beyond the static description, the classical and quantum free-energy profiles were obtained in two steps by using constrained *ab initio* MD and constrained centroid *ab initio* PIMD.[55,56] The constraint was implemented using the global proton-transfer coordinate $\Phi^T = \sum_{i=1}^{4} \phi_i/4$, where ϕ_i is the local reaction coordinate and is written as $\phi_i = d(D_iH_i)^{||} - d(A_iH_i)^{||}$.[45] $d(D_iH_i)^{||}$ ($d(A_iH_i)^{||}$) is the projection of the distance between the proton and the donor (acceptor) oxygen for the ith H bond denoted by $D - H \cdots A$ along the two in-plane axes of the simulation cell (detailed in the supplementary material). By integrating over the constraint forces, the free-energy profiles can be achieved.[45] During the MD and PIMD simulations, T was targeted at 50 K by the Andersen thermostat and a 0.2 fs time step was chosen. 48 replicas were used in the PIMD simulations. For more details about these computational setups, please see the supplementary material.

III. RESULTS

Water tetramers were constructed by manipulating four individual water monomers on the Au-supported NaCl(001) surface at 5 K with the Cl-terminated tip [Figs. 1(a) and 1(b)]. The chiral state of the cyclic water tetramer can be either clockwise state (CS) or anti-clockwise state (AS), which can be distinguished from the submolecular-resolution STM images [Figs. 1(c) and 1(e)]. In our previous work, we reported the direct visualization of the concerted proton tunneling in a water tetramer by monitoring the reversible interconversion of the two different H-bonding chiral states.[48] However, there is no experimental smoking gun for the concerted nature of proton tunneling. We notice that a breakdown of collective proton tunneling can be introduced by partial deuteration in fully quantum simulations of ice I_h.[46] Motivated by this, we moved a step further beyond our previous experimental study and directly measure the influence of partial isotopic substitution on the chirality switching of water tetramers.

These measurements were enabled by a recently developed tip-enhanced IETS technique, which allows us to distinguish individual H_2O and D_2O molecules by looking at the frequency of the O–H/D stretching mode [Fig. 1(g)].[28] This actually provides an unprecedented opportunity to construct partially and fully deuterated water tetramers in a well-controlled manner by replacing H_2O with D_2O one by one. The formation of the $3H_2O$+D_2O tetramer can be evidenced by the characteristic OH and OD vibrational features in the d^2I/dV^2 spectrum of the water tetramer [see the green curve in Fig. 1(g)]. Two vibrational peaks appeared around both the OH and OD stretching bands. One nearly coincides with that of the free OH(D) stretching and thus should arise from the upward free OH(D), while the other is red-shifted and should be attributed to the H(D)-bonded OH(OD). As a result, the constructed $3H_2O$+D_2O tetramer contains both free and bonded OH(D). The corresponding adsorption structures of two chiral $3H_2O$+D_2O tetramers are shown in Figs. 1(d) and 1(f).

The chirality of the water tetramer could be switched in a controlled manner with a Cl-terminated tip in close proximity to the tetramer [Fig. 2(a)], in such case the reaction barrier is effectively decreased owing to the tip-water electrostatic coupling.[48] The reversible interconversion of the tetramer chiralities can be monitored by recording the tunneling current, in which the two different levels correspond to the AS and CS of the tetramer, respectively [inset of Fig. 2(b)]. Multiple

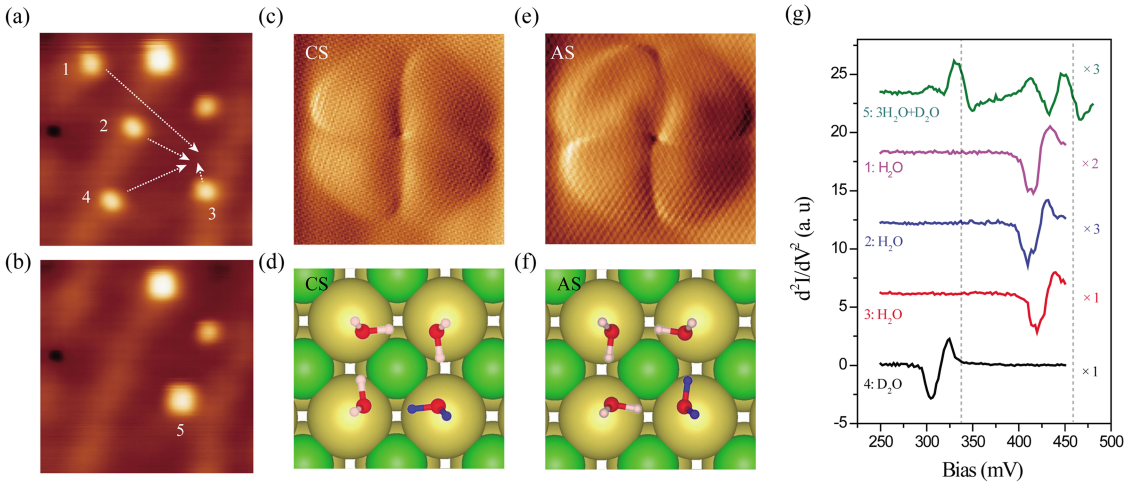

FIG. 1. Construction of a partial isotopic substituted water tetramer. [(a) and (b)] The construction of a water tetramer by manipulating three H_2O monomers (1,2,3) and one D_2O monomer (4) with a Cl-terminated tip at the set point of V = 10 mV and I = 150 pA. The white dashed arrows in (a) highlight the trajectories along which the water monomers were manipulated by the tip. The constructed tetramer is shown in (b). The size is 7.35 × 7.35 nm^2. Set point: V = 100 mV and I = 20 pA. [(c) and (e)] Derivative STM images of the water tetramers with clockwise state (CS) and anti-clockwise state (AS) H-bonded loops. The size is 1.3 × 1.3 nm^2. Set point: V = 10 mV and I = 90 pA (c), V = 10 mV and I = 100 pA (e). [(d) and (f)] Adsorption configuration of partially deuterated CS and AS tetramers, respectively. H, D, O, Cl^-, and Na^+ are denoted by pink, blue, red, green, and yellow spheres, respectively. (g) The d^2I/dV^2 spectra of the H_2O/D_2O monomers and partially deuterated water tetramer composed of three H_2O and one D_2O. Numbers 1 to 4 correspond to the water monomers shown in (a). The d^2I/dV^2 spectrum of the constructed $3H_2O$+D_2O tetramer is shown as a green curve. Here we focus on the stretching modes to tell the difference between D and H. Each curve is properly scaled to ensure the same magnitude for clarity. The vertical dashed lines denote the vibrational energies of the free OD (338 meV) and OH (460 meV) stretching modes. Set points of IETS: tip height: −240 pm, referenced to the set point: V = 100 mV and I = 20 pA (1,2,3,4); tip height: −290 pm, referenced to the set point: V = 100 mV and I = 50 pA (5).

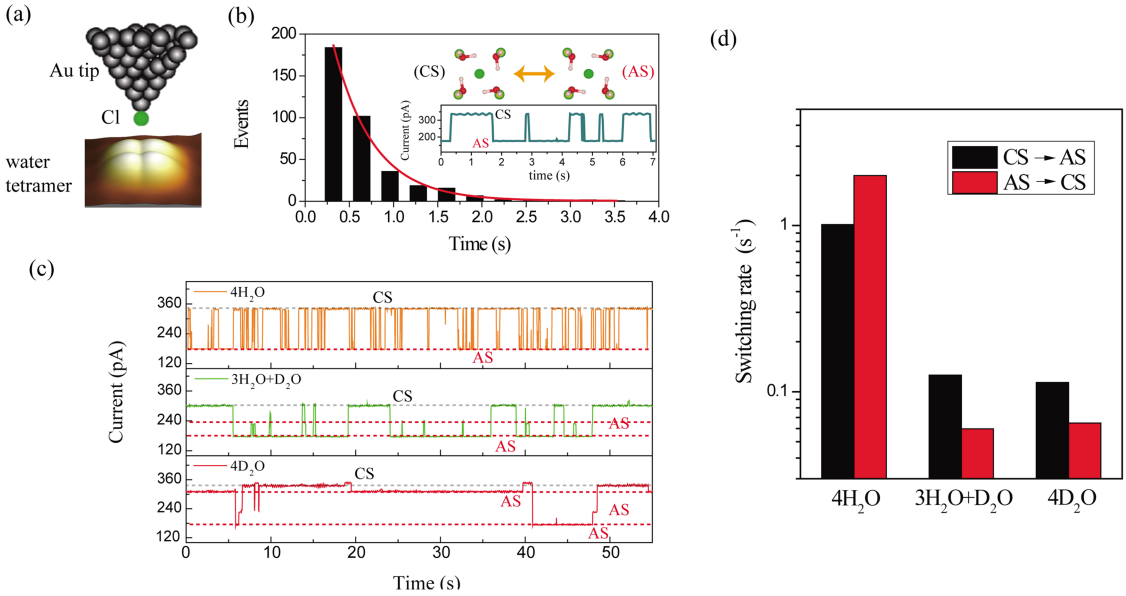

FIG. 2. Effect of full/partial isotopic substitution on the chirality switching of a water tetramer. (a) Schematic of the experimental setup using a Cl-tip. (b) Extraction of the switching rate from the current trace. The time distribution (bin size: 0.32 s) for the tetramer staying in the AS can be fitted to an exponential decay (red curve) based on the current trace (inset). The fitted time constant is 0.45 ± 0.031 s. The inverse of the time constant yields the switching rate: 2.22 ± 0.15 s^{-1}. Inset shows the adsorption configuration of CS and AS tetramers. [(c) and (d)] Current traces and the corresponding switching rates of the $4H_2O$, $3H_2O$+D_2O, and $4D_2O$ tetramers, respectively, during the chirality switching. The gray and red dashed lines represent the current levels for CS and AS of the tetramer, respectively. All the current traces were recorded at the same tip height of −265 pm, which is referenced to the gap set with: V = 5 mV and I = 5 pA.

current levels have also been observed due to the relaxation of the Cl-tip. However, no matter how many levels appear, they could be divided into two groups and each group corresponds to one of the two chiral states of the tetramer. Figure 2(b) shows the lifetime distribution of a anti-clockwise tetramer based on the inserted current trace, which could be well fitted to an exponential decay (red curve). The switching rate can be obtained by reversing the fitted time constant.

To explore the effect of full/partial isotopic substitution on the chirality switching of a water tetramer, we recorded the tunneling current traces of the $4D_2O$, $3H_2O$+D_2O, and $4D_2O$ tetramers, respectively, during the chirality switching [Fig. 2(c)]. Strikingly, the chirality switching rate of the $4H_2O$ tetramer is substantially reduced once by replacing only one H_2O with D_2O, almost to the same level of the $4D_2O$ tetramer [Fig. 2(d)]. This is in qualitative agreement with the prediction of the breakdown of concerted tunneling, as induced by a Zundel-like complex formed at the TS upon partial isotopic substitution of H by D in ice I_h.[46] Therefore, we consider this rapid quenching of the chirality switching of the partial deuterated water tetramer ($3H_2O$+D_2O) as a strong experimental support for the concerted proton tunneling in H_2O tetramers.

To better understand the atomistic details of the chirality switching between CS and AS, we now resort to *ab initio* theoretical simulations. At the atomic scale, the chirality switching of water tetramers can occur via different channels (modes). Stepwise proton transfer, intuitively the simplest process, has been investigated using the cNEB method in the supplementary material of Ref. 48. The formation of charged defects leads to a high reaction barrier (>2.0 eV). Therefore, we rule it out in the first place and focus on four other switching channels with lower barriers.

These four channels include collective proton transfer [inset of Fig. 3(a)], collective water molecule rotation involving one OH bond [inset of Fig. 3(b)], collective water molecule rotation involving two OH bonds [inset of Fig. 3(c)], and stepwise water molecule rotation [inset of Fig. 3(d)]. The reaction coordinates were chosen to be Φ^T and Φ^R, with Φ^T defined in Sec. II for the collective proton transfer and Φ^R used for the molecule rotations. We note that this Φ^R can be defined in the cNEB calculations after the relaxation of the intermediate sampling point along the reaction paths (detailed in the supplementary material). In the constrained MD/PIMD simulations, however, one needs to integrate out the fluctuation of the system on other degrees of freedom except the dimension of the system on the reaction coordinate in order to obtain an effective force. Technically, this is very difficult for the rotational channels. Therefore, we will discuss the cNEB results along Φ^T and Φ^R for these four channels first. Then the influence of NQEs on the barrier of the collective proton transfer channel will be analyzed by the thermodynamic integration (TI) method along Φ^T, when the effective forces and the free energies can be obtained. The influence of NQEs on other channels involving molecular rotations will be discussed later using an alternative estimator.

The cNEB barrier for the collective proton transfer is ~0.8 eV [Fig. 3(a)]. Collective rotations of four water molecules require apparently higher energies [>1.2 eV in Figs. 3(b) and 3(c)]. The stepwise rotation pathway, on the other hand, has the lowest barrier [Fig. 3(d)]. In this regard, the proton transfer in the water tetramer on the solid surface and in bulk ice show very different behaviors. In the classical limit, only defect-mediated single proton hopping occurs in ice I_h.[45] Whereas the stepwise water molecular rotation is the most favored channel for the rearrangement of the proton

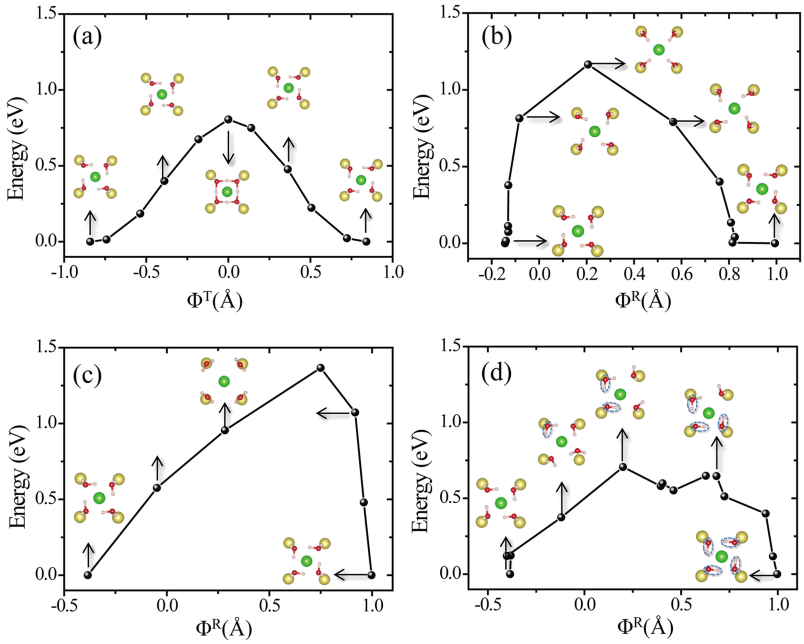

FIG. 3. Static energy profiles of the chirality switching in water tetramers via (a) collective proton transfer, collective rotations of four water molecules involving (b) one and (c) two OH bonds, and (d) step-wise rotation of four water molecules. The representative atomic structures along the reaction coordinates are shown as the insets. Yellow, green, red, and pink balls are Na, Cl, O, and H atoms, respectively. The water molecule switching sequences are indicated by the blue dashed circles in (d), for the step-wise rotation mode.

order in the water tetramer on the solid surface. The weaker special constraint of the H-bond network in the water tetramer, compared with that in bulk ice, is the main reason. This can be seen, e.g., by comparing the small barriers for molecular rotations in Figs. 2(b)–2(d) for the surface tetramer with that of the large barrier in Fig. S4 of the supplementary material for the hexagonal ring in ice I_h.

Now we include nuclear statistical effects at the classical and quantum levels. This is done by performing comparative *ab initio* MD and PIMD simulations. The TI method was used to obtain free energy profiles due to the rare-event nature of this process, by constraining the global reaction coordinate Φ^T at various values.[55,56] Φ^T can quantitatively describe the progress of the collective four-proton transfer in the water tetramer. Free energies as a function of Φ^T with classical and quantum nuclei are shown in Fig. 4. *Ab initio* MD simulations at 50 K give a barrier of ~0.73 eV, similar to the static result from cNEB, meaning that the classical thermal effects are small.

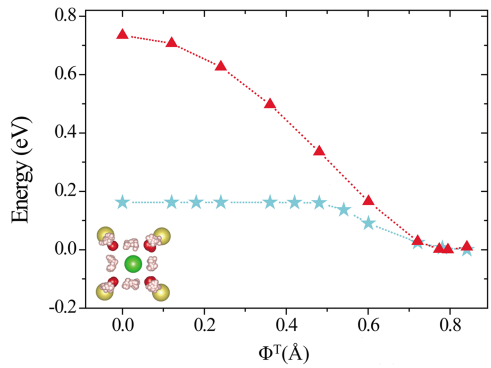

FIG. 4. Free-energy profiles obtained with *ab initia* constrained MD (red triangles) and PIMD (cyan stars) simulations for the concerted proton transfer in the water tetramer on the NaCl(001) surface at 50 K. A PIMD simulation snapshot for the TS is shown as the inset. Red and pink balls represent the beads of O and H atoms, for one snapshot in a PIMD simulation. The centroids of Na and Cl atoms are shown as yellow and green balls.

The corresponding scenario is that the collective proton transfer happens through thermal hopping, which is a very rare event. With quantum nuclei, however, we see a substantially reduced energy barrier (~0.16 eV). The value of reduction is much larger than the zero-point energy corrections. Therefore, quantum tunneling should play the most important role. This translational quantum tunneling can also be reflected in the snapshot of the constrained-centroid PIMD simulations at the TS (Fig. 4), where the quantum path (circular ring of each nucleus) is obviously delocalized toward its initial and final states. Later, we will discuss the bimodal structure of this distribution, which is a clear evidence of deep tunneling. The NQEs also play an important role on the collective proton transfers in the $3H_2O$+D_2O and $4D_2O$ tetramers. The profiles of the mean constrained forces are shown in Fig. S2 of the supplementary material. The quantum free energy barrier is ~0.18 eV for $3H_2O$+D_2O and ~0.22 eV for $4D_2O$.

For the molecular rotation modes, as mentioned, it is technically difficult to control the systems going from CS to AS by gradually changing an appropriate global reaction coordinate, meaning that we cannot obtain the free energy profiles with the TI method. An alternative estimator, therefore, must be resorted to. Based on the cNEB calculations, we plot the static energy profiles for various chirality switching channels in Fig. 5. Then, we constrained the centroid of each atom at the spatial configuration obtained from cNEB in the PIMD simulations for each intermediate state and calculated the thermodynamic averages of the total energy using the virial energy estimator.[35] This virial energy is defined as

$$E = \langle \frac{\hat{p}^2}{2m} + U(\hat{x}) \rangle = \frac{3Nk_BT}{2} + \frac{1}{P}\sum_{k=1}^{P}\sum_{i=1}^{N}\frac{1}{2}(\mathbf{r}_i^k - \mathbf{r}_i^c)\cdot\frac{\partial U}{\partial \mathbf{r}_i^k} + \frac{1}{P}\sum_{k=1}^{P} U(r_1^k, \ldots, r_N^k),$$

where P is the number of the beads in PIMD simulations, N is the number of ions, U is the potential energy on the

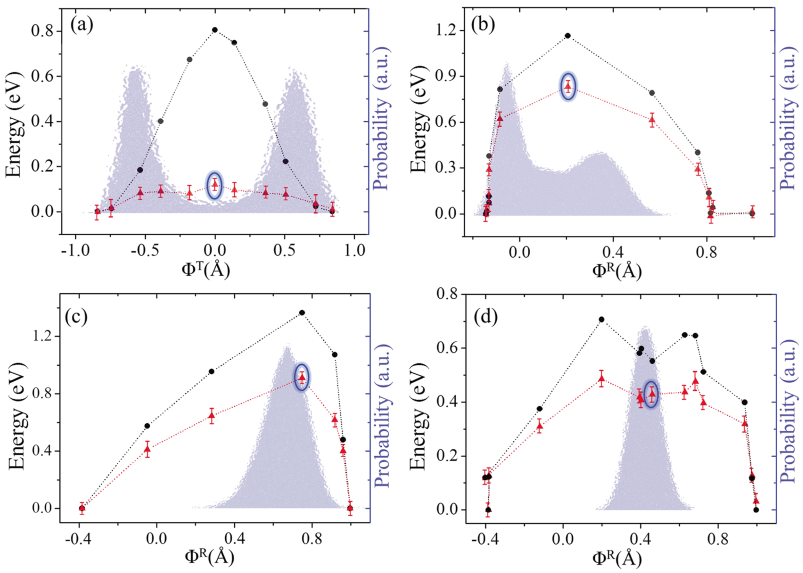

FIG. 5. Energy profiles from cNEB calculations (black dots) and PIMD simulations (red triangles), for four kinds of water chirality switching modes as shown in Fig. 3. In each PIMD simulations, the centroids of atoms are constrained at the positions of corresponding cNEB image states. The distribution probabilities of reaction coordinates are also shown by shades in each figure for the TSs.

Bohn-Oppenheimer surface, $\mathbf{r}_i^k$ is the position of the kth bead of ion i, and $\mathbf{r}_i^c$is the centroid of ion i. With this treatment, we acknowledge that contributions from entropy to the free energy cannot be taken into account. The constraint of the pathway also means that the well-known corner cutting effects are absent since the quantum tunneling path can be very different from the classical one.[62–64] The averaged virial energy profiles at 50 K are shown in Fig. 5, along with the static energy profiles, for the four chirality switching channels. For collective proton transfer, the barrier of the virial energy is ~0.12 eV [Fig. 5(a)]. This value is much smaller than the static energy and the classical free energy barriers. It is also close to the quantum free energy barrier (~0.16 eV). This close value between the quantum virial total energy and the quantum free energy indicates that it is reasonable to evaluate the role of NQEs on this chirality switching problem using the virial estimator.

Now we investigate the NQEs on other chirality switching channels. In contrast to the substantial reduction of the switching barrier due to NQEs for collective proton transfer, NQEs on the molecule rotation channels are much weaker. This is shown in Figs. 5(b)–5(d), where the virial energy barriers are still very high. To understand this, we plot the distribution probabilities of the path-integral images as a function of the reaction coordinates (Φ^T and Φ^R) at the TSs (indicated by blue circles) and show these distributions by shades in Fig. 5. For collective proton transfer, obvious proton delocalization between the two degenerate states along H-bonds can be seen and deep tunneling plays an important role at 50 K. This is consistent with Ref. 45 for the hexagonal H-bonded ring in bulk ice I_h. For the molecular rotation modes, however, this delocalization is much weaker. As a matter of fact, bimodal distribution only exists for the molecular rotation involving one OH bond [Fig. 5(b)]. And this bimodal feature is much weaker than that of the collective proton tunneling in Fig. 5(a). In Figs. 5(c) and 5(d), this delocalization does not even exist.

For a more direct visualization of the difference between the quantum delocalization along each channel, we take two of them as examples when this delocalization happens and show some representative snapshots of the constrained-centroid PIMD simulations in Fig. 6. These two channels include the collective proton transfer [Fig. 5(a)] and the collective rotation involving one OH bond [Fig. 5(b)]. Different from the shades in Fig. 5 where only the imaginary-time images at the TS were taken into the statistics, three intermediate states were chosen along each reaction path in Fig. 6 to represent the state of the tetramer before, during, and after the chirality switching. The proton delocalization between the two degenerate states can still be seen for both channels at the TSs [Figs. 6(b) and 6(e)]. This is in agreement with the probability distributions for Φ^T and Φ^R in Figs. 5(a) and 5(b). For the collective proton transfer channel, such delocalization can also be seen within a wide range of Φ^T [Figs. 6(a) and 6(c)]. This results in a nearly flat terrace in the free energy and the virial energy profiles around the TS in Figs. 4 and 5(a). For the collective rotation channel involving one OH bond, delocalization occurs only near the TS [Fig. 6(e)]. Before and after this TS,

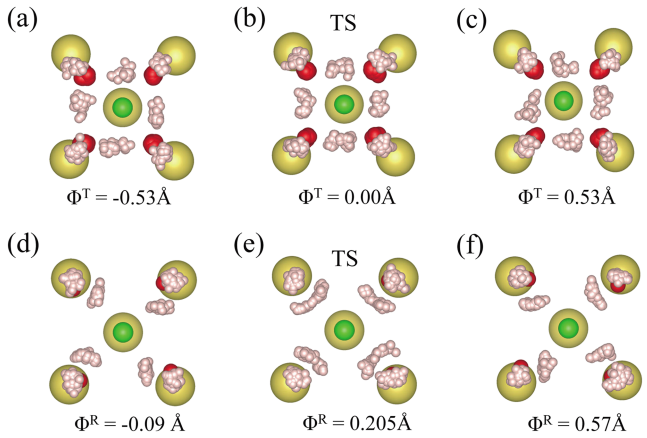

FIG. 6. The representative snapshots during the constrained-centroid PIMD simulations with different reaction coordinates. [(a)–(c)] Concerted proton tunneling. [(d)–(f)] Collective water rotation. Red and pink balls represent the beads of O and H atoms. The centroids of Na and Cl atoms are shown as yellow and green balls.

the imaginary paths of the transferring protons are quite localized [Figs. 6(d) and 6(f)], which explains the weaker influence of NQEs on the virial energy profile. In short, NQEs have very different influences on the four chirality switching channels. Although the stepwise rotation channel [Fig. 3(d)] is the most facile way to accomplish the chirality switching in the classical limit, deep quantum tunneling puts the collective proton transfer channel in a much more favorable position at low T.

The computed classical and quantum free energy barriers for concerted proton transfer can be further used to estimate the chirality switching rates with the quantum transition-state theory (QTST) method.[35,36,65–67] Due to the principles of quantum mechanics, a quantum analogue of the classical transition state theory (TST) cannot be rigorously defined.[65–67] However, huge benefits exist in estimations of the rate constants with NQEs in terms of tunneling and zero-point motion accounted for without necessarily calculating the quantum real time dynamics. This makes existing versions of QTST extremely valuable in simulations of large polyatomic systems.[68–73] Here we adopt a practical version in which the rate is calculated by $k_{QTST} = \frac{\bar{\nu}}{2} P\left(\xi^{\#}, T\right) = \frac{\bar{\nu}}{2} P\left(\xi^{0}, T\right) e^{-\Delta F/k_B T}$, where $\bar{\nu}$ is written as $\bar{\nu} = (2k_B T/\pi m)^{1/2}$.[72] $P\left(\xi^{\#}, T\right)$ and $P\left(\xi^{0}, T\right)$ are the centroid (center of mass of the ring polymer) probability densities at the transition state $\xi^{\#}$ and initial state ξ^{0}, and ΔF is the free-energy barrier for the concerted proton tunneling. This expression satisfies the requirement that classical TST is recovered at the classical limit.

The computed classical and quantum rates as a function of the temperature are shown in Fig. 7. The calculated switching rates at 50 K for $4H_2O$, $3H_2O$+D_2O, and $4D_2O$ systems are 4.58×10^{-3} s^{-1}, 4.92×10^{-5} s^{-1}, and 1.85×10^{-8} s^{-1} respectively. The turnover between the classical hopping and the quantum tunneling regions is clear. The experimental measurement of the switching rates and isotope effects were qualitatively reproduced. In particular, partial deuteration of the water tetramer ($3H_2O$+D_2O) can lead to more than two orders of magnitude drop in the switching rate, which is consistent with the experimental observation. However, we note that the computed switching rate at 50 K is quantitatively inaccurate in general, much lower than the measured rates of ~1 s^{-1} [Fig. 2(d)], and the calculated isotope effects are larger than our experimental observations. Besides this, although partial deuteration leads to two orders of magnitude decrease of the chirality switching rate, it does not give a value comparable to full deuteration. Considering the facts that our simulations were performed at 50 K (higher than the experimental temperature of ~5 K), various density functionals will result in slightly different cNEB barriers for the collective proton tunneling as shown in Table S1 of the supplementary material, the Au tip is not employed in the simulation model, and the symmetry of coupling between the Cl anion and the four protons may also play an important role,[48] we will leave better quantitative interpretations of the experimental rates as a topic for future studies.

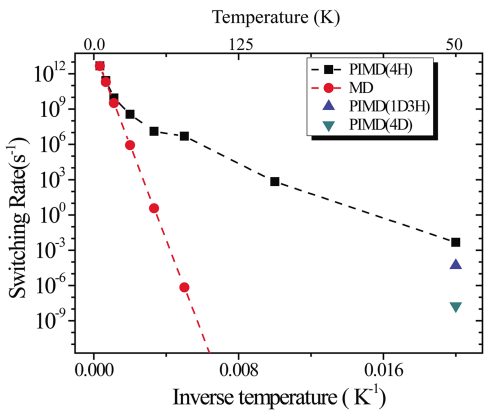

FIG. 7. The temperature dependence of chirality switching rates. Red and black dashed lines represent the calculated classical and quantum switching rates of $4H_2O$ tetramer, respectively. Blue up-triangle and green down-triangle are calculated switching rates for $3H_2O$+$1D_2O$ and $4D_2O$ tetramers with PIMD at 50 K.

IV. CONCLUSIONS AND DISCUSSIONS

In short, we report here a combined experimental and theoretical study on the chirality switching of the water tetramer on the NaCl(001) surface. Experimentally, we found that upon partial deuteration of water tetramer, the switching rate is seriously reduced. This provides a direct experimental support for the breakdown of the concerted proton tunneling mechanism upon partial deuteration as suggested in an earlier quantum simulation for ice I_h. Using classical and quantum *ab initio* simulations, we then compared different switching modes including concerted proton tunneling and collective/stepwise water molecule rotations. Static barriers obtained using cNEB show that the stepwise rotation of water molecules is the most facile one in the classical limit. *Ab initio* PIMD, however, gives a much lower barrier (<0.2 eV) for collective transferring than other channels at 50 K. This is due to the fact that NQEs have different influences on each chirality switching mode. Obvious delocalization plays a more important role for collective proton tunneling. Using one practical version of QTST, we calculated the T-dependent chirality switching rates and the isotope effects, which qualitatively explained the experimental observations.

Given the fundamental importance of quantum tunneling in the dynamics of H-bonded systems, these results have a number of implications. The high dimensionality of realistic H-bonded system and the topology of H-bond network mean that collective proton tunneling may exist more ubiquitously than expected not only in bulk ice[45–48] but also in gas phase clusters[40–43,73] and on surfaces.[39,48] One advantage of the surface systems is that they are easily accessible to high-resolution experimental measurements. Therefore, we believe systems of this kind can provide ideal platforms for future experimental studies of this mechanism. Theoretically, the high dimensionality of realistic systems also means that the effective forces could be difficult to be obtained in the TI simulations. The virial energy used here provides a reasonable estimator for the description of the NQEs when the TI method cannot be applied, which may be employed in future studies of similar problems. However, we completely acknowledge that the absence of entropic effects and corner-cutting effects also means that its validity cannot be guaranteed and must be checked for each

application. Higher level quantum dynamics methods, such as on-the-fly instanton, centroid molecular dynamics,[74,75] ring-polymer molecular dynamics,[76,77] and path-integral Louvielle dynamics,[78] are highly desired in descriptions of these phenomena. We hope our work can stimulate more research on collective tunneling in this direction.

SUPPLEMENTARY MATERIAL

See supplementary material for details of the experimental setup and additional information of the theoretical simulations.

ACKNOWLEDGMENTS

This work was supported by the National Key R&D Program under Grant Nos. 2016YFA0300901 and 2017YFA0205003, the National Basic Research Programs of China under Grant No. 2013CB934600, the National Natural Science Foundation of China under Grant Nos. 11422431, 11774003, 11275008, 11634001, 11604092, 11274002, 91021007, and 11290162/A04010. Y.J. acknowledges support by the National Science Fund for Distinguished Young Scholars and Cheung Kong Young Scholar Program. J.G. acknowledges support from the National Postdoctoral Program for Innovative Talents. We are grateful for the computational resources provided by the supercomputer TianHe-1A in Tianjin, China.

[1] J. D. Watson and F. H. C. Crick, Nature **171**, 964 (1953).
[2] M. Elstner, P. Hobza, T. Frauenheim, S. Suhai, and E. Kaxiras, J. Chem. Phys. **114**, 5149 (2001).
[3] W. Fang, J. Chen, M. Rossi, Y. X. Feng, X. Z. Li, and A. Michaelides, J. Phys. Chem. Lett. **7**, 2125 (2016).
[4] C. J. Pickard, M. Martinez-Canales, and R. J. Needs, Phys. Rev. Lett. **110**, 245701 (2013).
[5] M. Benoit, D. Marx, and M. Parrinello, Nature **392**, 258 (1998).
[6] Y. Wang, H. Liu, J. Lv, L. Zhu, H. Wang, and Y. Ma, Nat. Commun. **2**, 563 (2011).
[7] J. Sun, B. K. Clark, S. Torquato, and R. Car, Nat. Commun. **6**, 8156 (2015).
[8] L. R. Merte, G. Peng, R. Bechstein, F. Rieboldt, C. A. Farberow, L. C. Grabow, W. Kudernatsch, S. Wendt, E. Lægsgaard, and M. Mavrikakis, Science **336**, 889 (2012).
[9] S. Hu, M. Lozada-Hidalgo, F. C. Wang, A. Mishchenko, F. Schedin, R. R. Nair, E. W. Hill, D. W. Boukhvalov, M. I. Katsnelson, R. A. Dryfe, I. V. Grigorieva, H. A. Wu, and A. K. Geim, Nature **516**, 227 (2014).
[10] M. Lozada-Hidalgo, S. Hu, O. Marshall, A. Mishchenko, A. Grigorenko, R. Dryfe, B. Radha, I. Grigorieva, and A. Geim, Science **351**, 68 (2016).
[11] Y. X. Feng, J. Chen, W. Fang, E. G. Wang, A. Michaelides, and X. Z. Li, e-print arXiv:1704.00914v2.
[12] A. Kohen and J. P. Klinman, Acc. Chem. Res. **31**, 397 (1998).
[13] A. Kohen, R. Cannio, S. Bartolucci, and J. P. Klinman, Nature **399**, 496 (1999).
[14] Z. X. Liang and J. P. Klinman, Curr. Opin. Struct. Biol. **14**, 648 (2004).
[15] L. Masgrau, K. E. Ranaghan, N. S. Scrutton, A. J. Mulholland, and M. J. Sutcliffe, J. Phys. Chem. B **111**, 3032 (2007).
[16] L. Masgrau, A. Roujeinikova, L. O. Johannissen, P. Hothi, J. Basran, K. E. Ranaghan, A. J. Mulholland, M. J. Sutcliffe, N. S. Scrutton, and D. Leys, Science **312**(5771), 237–241 (2006).
[17] J. B. Rommel, Y. Liu, H. J. Werner, and J. Kästner, J. Phys. Chem. B **116**, 13682 (2012).
[18] M. E. Tuckerman, D. Marx, M. L. Klein, and M. Parrinello, Science **275**, 817 (1997).
[19] M. Ceriotti and D. E. Manolopoulos, Phys. Rev. Lett. **109**, 100604 (2012).
[20] J. A. Morrone and R. Car, Phys. Rev. Lett. **101**, 017801 (2008).
[21] R. Ramírez, P. P. Kumar, and D. Marx, J. Chem. Phys. **121**, 3973 (2004).
[22] F. Paesani, S. Iuchi, and G. A. Voth, J. Chem. Phys. **127**, 074506 (2007).
[23] S. Habershon, G. S. Fanourgakis, and D. E. Manolopoulos, J. Chem. Phys. **129**, 074501 (2008).
[24] M. Ceriotti, J. Cuny, M. Parrinello, and D. E. Manolopoulos, Proc. Natl. Acad. Sci. U. S. A. **110**, 15591 (2013).
[25] S. Habershon, T. E. Markland, and D. E. Manolopoulos, J. Chem. Phys. **131**, 024501 (2009).
[26] X. Z. Li, B. Walker, and A. Michaelides, Proc. Natl. Acad. Sci. U. S. A. **108**, 6369 (2011).
[27] M. Ceriotti, W. Fang, P. G. Kusalik, P. H. McKenzie, A. Michaelides, M. A. Morales, and T. E. Markland, Chem. Rev. **116**, 7529 (2016).
[28] J. Guo, J.-T. Lü, Y. Feng, J. Chen, J. Peng, Z. Lin, X. Meng, Z. Wang, X. Z. Li, E. G. Wang, and Y. Jiang, Science **352**, 321 (2016).
[29] C. J. D. von Grotthuss, Ann. Chim. **LVIII**, 54 (1806).
[30] D. Marx, ChemPhysChem **7**, 1848 (2006).
[31] X. Z. Li, M. I. J. Probert, A. Alavi, and A. Michaelides, Phys. Rev. Lett. **104**, 066102 (2010).
[32] J. A. Morrone, L. Lin, and R. Car, J. Chem. Phys. **130**, 204511 (2009).
[33] W. H. Miller, J. Chem. Phys. **61**, 1823 (1974).
[34] W. H. Miller, Y. Zhao, M. Ceotto, and S. Yang, J. Chem. Phys. **119**, 1329 (2003).
[35] I. R. Craig and D. E. Manolopoulos, J. Chem. Phys. **122**, 84106 (2005).
[36] I. R. Craig and D. E. Manolopoulos, J. Chem. Phys. **123**, 034102 (2005).
[37] J. O. Richardson and S. C. Althorpe, J. Chem. Phys. **131**, 214106 (2009).
[38] Y. Li, Y. V. Suleimanov, W. H. Green, and H. Guo, J. Phys. Chem. A **118**, 1989 (2014).
[39] M. Koch, M. Pagan, M. Persson, S. Gawinkowski, J. Waluk, and T. Kumagai, J. Am. Chem. Soc. **139**, 12681 (2017).
[40] S. Nagaoka, T. Terao, F. Imashiro, A. Saika, N. Hirota, and S. Hayashi, J. Chem. Phys. **79**, 4694 (1983).
[41] A. J. Horsewill and A. Albout, J. Phys.: Condens. Matter **1**, 9609 (1989).
[42] V. A. Benderskii, S. Y. Grebenshchikov, D. E. Makarov, and E. V. Vetoshkin, Chem. Phys. **185**, 101 (1994).
[43] F. Madeja and M. Havenith, J. Chem. Phys. **117**, 7162 (2002).
[44] L. E. Bove, S. Klotz, A. Paciaroni, and F. Sacchetti, Phys. Rev. Lett. **103**, 165901 (2009).
[45] C. Drechsel-Grau and D. Marx, Phys. Rev. Lett. **112**, 148302 (2014).
[46] C. Drechsel-Grau and D. Marx, Angew. Chem., Int. Ed. **53**, 10937 (2014).
[47] C. Dreschsel-Grau and D. Marx, Phys. Chem. Chem. Phys. **19**, 2623 (2017).
[48] X. Meng, J. Guo, J. Peng, J. Chen, Z. Wang, J.-R. Shi, X.-Z. Li, E.-G. Wang, and Y. Jiang, Nat. Phys. **11**, 235 (2015).
[49] J. Guo, X. Meng, J. Chen, J. Peng, J. Sheng, X.-Z. Li, L. Xu, J.-R. Shi, E. Wang, and Y. Jiang, Nat. Mater. **13**, 184 (2014).
[50] C. Drechsel-Grau and D. Marx, Nat. Phys. **11**, 216 (2015).
[51] G. Kresse and J. Hafner, Phys. Rev. B **47**, 558 (1993).
[52] G. Kresse and J. Hafner, Phys. Rev. B **49**, 14251 (1994).
[53] J. Chen, X. Z. Li, Q. F. Zhang, M. I. J. Probert, C. J. Pickard, R. J. Needs, A. Michaelides, and E. G. Wang, Nat. Commun. **4**, 2064 (2013).
[54] Y. X. Feng, J. Chen, D. Alfè, X. Z. Li, and E. G. Wang, J. Chem. Phys. **142**, 064506 (2015).
[55] M. E. Tuckerman and D. Marx, Phys. Rev. Lett. **86**, 4946 (2001).
[56] B. Walker and A. Michaelides, J. Chem. Phys. **133**, 174306 (2010).
[57] D. Marx and M. Parrinello, Z. Phys. B: Condens. Matter **95**, 143 (1994).
[58] D. Marx and M. Parrinello, Nature **375**, 216 (1995).
[59] D. Marx and M. Parrinello, J. Chem. Phys. **104**, 4077 (1996).
[60] M. E. Tuckerman, D. Marx, M. L. Klein, and M. Parrinello, J. Chem. Phys. **104**, 5579 (1996).
[61] G. Henkelman, B. P. Uberuaga, and H. Jónsson, J. Chem. Phys. **113**, 9901 (2000).
[62] R. A. Marcus and M. E. Coltrin, J. Chem. Phys. **67**, 2609 (1977).
[63] R. T. Skodje, D. G. Truhlar, and B. C. Garrett, J. Chem. Phys. **77**, 5955 (1982).
[64] A. Fernandez-Ramos and D. G. Truhlar, J. Chem. Phys. **114**, 1491 (2001).
[65] W. H. Miller, Acc. Chem. Res. **26**, 174 (1993).
[66] F. J. McLafferty and P. Pechukas, Chem. Phys. Lett. **27**, 511 (1974).
[67] S. J. Jang and G. A. Voth, J. Chem. Phys. **146**, 174106 (2017).
[68] M. Tuckerman, *Statistical Mechanics: Theory and Molecular Simulation* (Oxford University Press, 2010).
[69] G. Mills, G. K. Schenter, D. E. Makarov, and H. Jonsson, Chem. Phys. Lett. **278**, 91 (1997).
[70] Q. Zhang, G. Wahnstrom, M. E. Bjorketun, S. Gao, and E. G. Wang, Phys. Rev. Lett. **101**, 215902 (2008).

[71] W. Fang, J. O. Richardson, J. Chen, X. Z. Li, and A. Michaelides, Phys. Rev. Lett. **119**, 126001 (2017).
[72] E. M. McIntosh, K. T. Wikfeldt, J. Ellis, A. Michaelides, and W. Allison, J. Phys. Chem. Lett. **4**, 1565 (2013).
[73] J. O. Richardson, C. Pérez, S. Lobsiger, A. A. Reid, B. Temelso, G. C. Shields, Z. Kisiel, D. J. Wales, B. H. Pate, and S. C. Althorpe, Science **351**, 1310 (2016).
[74] J. Cao and G. A. Voth, J. Chem. Phys. **100**, 5106 (1994).
[75] S. Jang and G. A. Voth, J. Chem. Phys. **111**, 2371 (1999).
[76] I. R. Craig and D. E. Manolopoulos, J. Chem. Phys. **121**, 3368 (2004).
[77] S. Habershon, D. E. Manolopoulos, T. E. Markland, and T. F. Miller III, Annu. Rev. Phys. Chem. **64**, 387 (2013).
[78] J. Liu, J. Chem. Phys. **140**, 224107 (2014).